Simulated Two-Stage Recovery of Atlantic Meridional Overturning Circulation During the Last Deglaciation

Jun Cheng,[1] Zhengyu Liu,[2,3] Feng He,[2] Bette L. Otto-Bliesner,[4] Esther C. Brady,[4] and Mark Wehrenberg[2]

A two-stage recovery of Atlantic meridional overturning circulation (AMOC) during Bølling Allerød (BA) is revealed in the first transient simulation of last deglaciation in a fully coupled general circulation model (Transient Simulation of Climate Evolution over the Last 21,000 Years (TraCE-21000)). After being suppressed during the Heinrich 1 event, North Atlantic Deep Water (NADW) formation first reinitiates in the Labrador Sea in stage 1 and then reinitiates in the Greenland-Iceland-Norwegian (GIN) seas in stage 2. This feature is derived from the investigation of NADW formation in its two origins with a newly developed method and is confirmed by the comprehensive analysis of relative variables. A new mechanism is proposed to interpret the northward asynchronous reinitiation of NADW during BA. In addition, our work also points out that the generation of the AMOC overshoot is associated with the reinitiation of NADW in GIN seas.

1. INTRODUCTION

Paleoclimate records and climate model simulations suggest that climate change on centurial-millennial time scales is largely connected with the variation of Atlantic meridional overturning circulation (AMOC) [*Broecker*, 1990; *Manabe and Stouffer*, 1995; *Vellinga and Wood*, 2002; *Levermann et al.*, 2005]. In addition to the slowdown/shutdown of AMOC, sometimes the pronounced abrupt climate change is also associated with AMOC recovery after fresh meltwater discharge in the North Atlantic [*Ganopolski and Rahmstorf*, 2001; *Rahmstorf*, 2002; *Clarke et al.*, 2002; *McManus et al.*, 2004; *Lippold et al.*, 2009]. In the first transient simulation of the last deglaciation with a fully coupled model (Transient Simulation of Climate Evolution over the Last 21,000 Years (TraCE-21000)), the abrupt onset of Bølling Allerød (BA) warming was captured, and it was found that the onset of BA warming is dominated by the recovery of the AMOC. A 10°C air temperature increase over Greenland during BA onset accompanies a 16.5 Sv increase of AMOC intensity within 300 years [*Liu et al.*, 2009].

The details of the recovery process of AMOC have not been fully explained in the literature so far. Some studies simply define one latitude band in the North Atlantic as the important North Atlantic Deep Water (NADW) formation region to explain AMOC recovery and do not consider the details of NADW reinitiation in multiple origins [*Krebs and Timmermann*, 2007a, 2007b; *Hu et al.*, 2007; *Mignot et al.*, 2007]. This simplified method relies upon two points: (1) the low resolution of the ocean model that employed a longer integration for AMOC study and (2) the broad convection area in the model simulation that was not only limited to the

[1]Key Laboratory of Meteorological Disaster of Ministry of Education and College of Atmospheric Sciences, Nanjing University of Information Science and Technology, Nanjing, China.

[2]Center for Climatic Research and Department of Atmospheric and Oceanic Sciences, University of Wisconsin-Madison, Madison, Wisconsin, USA.

[3]Also at Laboratory for Climate and Ocean-Atmosphere Studies and Department of Atmospheric and Oceanic Sciences, Peking University, Beijing, China.

[4]Climate and Global Dynamics Division, National Center for Atmospheric Research, Boulder, Colorado, USA.

Abrupt Climate Change: Mechanisms, Patterns, and Impacts
Geophysical Monograph Series 193

10.1029/2010GM001014

Labrador Sea or the Greenland-Iceland-Norwegian (GIN) seas. Despite the dependence of model formulation and internal variability of the AMOC fluctuation under control runs, the AMOC changes in perturbation experiments (water-hosing experiments) are mainly associated with the convection changes in the Labrador Sea and GIN seas with asynchronous and different contributions [*Krebs and Timmermann*, 2007a, 2007b; *Mignot et al.*, 2007; *Vellinga and Wood*, 2002]. This mechanism of AMOC variability is found in the widely used Community Climate System Model version 3 (CCSM3) under control and water-hosing experiments in glacial, preindustrial, and present-day climate conditions [*Hu et al.*, 2007; *Renold et al.*, 2009]. So the details of NADW reinitiation in multiple areas of origin are important for the understanding of the AMOC recovery process. Other works have touched upon the asynchronicity of the reinitiation of deepwater formation at different locations, but these studies provide divergent conclusions. Starting with an artificially "turned off" state of AMOC in model HadCM3 under modern climate conditions, *Vellinga and Wood* [2002] found that NADW formation reinitiates first in the GIN seas and then moves southward to the Labrador Sea. This work also proposed that the northward salt transport determines the order of the NADW reinitiation. In contrast, *Renold et al.* [2009] found that the reinitiation of the NADW first occurred in the Labrador Sea and then in the GIN seas, based on a series of water-hosing experiments with CCSM3. Renold et al. proposed that the northward salt and heat transport determines the northward reinitiation of NADW beneath the retreat of sea ice. The contradictory results of *Vellinga and Wood* [2002] and *Renold et al.* [2009] rely upon the attendance of sea ice change during the AMOC recovery period and maybe the dependence of the models. However, the results of *Renold et al.* [2009] seem to simulate the real world more closely because of the more realistic experiment scheme.

Renold et al. [2009] also found two stages in the recovery of AMOC, as suggested by the evolutionary characteristics of the AMOC intensity. However, in many studies using different models with different complexities, a two-stage mechanism of AMOC recovery is not always evident in a single time series of AMOC intensity [*Manabe and Stouffer*, 1997; *Knutti et al.*, 2004; *Mignot et al.*, 2007; *Arzel et al.*, 2008]. The two-stage feature of AMOC recovery seems to rely on the asynchronicity of NADW reinitiation in multiple origins according to *Renold et al.* [2009]. The asynchronous feature of the NADW reinitiation in multiple origins could induce the intensity series to present the two-stage feature but may not always do so. This suggests that a single measure of AMOC intensity maybe not be a good choice for judging whether the reinitiation of NADW in multiple origins is asynchronous or not. A detailed investigation of the AMOC recovery process should take a broader view of the geographical heterogeneity of the NADW formation in the North Atlantic and the regional contributions to the total AMOC intensity.

Another deficiency in studies of the AMOC recovery is that idealized water-hosing experiments are not typically run for long enough to study the entire recovery process. Previous modeling studies usually emphasized the prerecovery period of the simulation, ending when the AMOC intensity resumes its unperturbed level for the first time and neglecting whether the AMOC system has fully recovered or not [*Vellinga and Wood*, 2002; *Bitz et al.*, 2007; *Hu et al.*, 2008; *Renold et al.*, 2009]. Actually, numerous experiments with different models have shown that the AMOC will keep increasing after its initial recovery and continue to increase in intensity before returning to its unperturbed level, exhibiting an "overshoot" phenomenon [*Manabe and Stouffer*, 1997; *Knutti et al.*, 2004; *Stouffer et al.*, 2006; *Mignot et al.*, 2007; *Krebs and Timmermann*, 2007a, 2007b; *Schmittner and Galbraith*, 2008; *Arzel et al.*, 2008; *Liu et al.*, 2009]. The historic occurrence of an AMOC overshoot during the BA event has been validated with combined observational and model evidence. That this is the effect of AMOC overshoot in deep currents of the North Atlantic regionally is shown in model simulations, and this feature is consistent with the distribution of reconstructed proxies such as cores GGC5 and TTR-451 (J. Cheng et al., Model-proxy comparison for overshoot phenomenon of Atlantic thermohaline circulation at Bølling-Allerød, unpublished manuscript, 2011). So the postrecovery stage, or overshoot stage, of the AMOC system should not be ignored.

The mechanisms for AMOC recovery are still not well understood. With an intermediate complexity model (CLIMBER-3α), *Wright and Stocker* [1991] and *Mignot et al.* [2007] thought the recovery of AMOC derived from the destabilized stratification with warmed abyssal water in the North Atlantic. Using the intermediate complexity model ECBILT-CLIO, *Goosse et al.* [2002] proposed that the recovery of AMOC comes from a stochastic process of air-sea interaction. With a coupled general circulation model (GCM) such as LSG-ECHAM3/T42, *Knorr and Lohmann* [2003] proposed that a weakened Antarctic Bottom Water cell contributes to the recovery of AMOC. With different complexity models, *Vellinga and Wood* [2002] (HadCM3 and coupled GCM), *Yin et al.* [2006] (UIUC and coupled GCM), and *Krebs and Timmermann* [2007a, 2007b] (intermediate complexity model and ECBILT-CLIO) hypothesized that the northward advection of the salinity anomaly is the key factor for AMOC recovery, and this hypothesis is supported by paleorecords [*Carlson et al.*, 2008].

Because of our lack of understanding of the dominant processes underlying past shifts in the AMOC and the increasing research interest in global warming in the past [*Carlson et al.*, 2008; *Milne and Mitrovica*, 2008; *Barker et al.*, 2009; *Liu et al.*, 2009], a detailed investigation of the processes controlling AMOC recovery during the last deglaciation is still needed. TraCE-21000 simulation provides a basis to address this issue [*Liu et al.*, 2009]. This simulation focus on a historic global warming period (last deglaciation) and its results should be helpful to understand the more general processes controlling AMOC variation and to project the future behavior of possible AMOC changes under current and projected global warming.

In this study, we investigate the recovery process of AMOC during BA onset in TraCE-21000 simulation, emphasizing the processes underlying the reinitiation of NADW in its two origins. A detailed analysis of surface and subsurface variables provides a framework for discussing the different stages involved in the AMOC recovery process. A description of the model and simulation setup is given in section 2. The two-stage feature of AMOC recovery is presented in section 3, while the processes underlying the recovery stages are discussed in section 4. Discussion and conclusions follow in section 5.

2. MODEL AND EXPERIMENTAL SETUP

The CGCM used in this study is the National Center for Atmospheric Research (NCAR) CCSM3 with a dynamic global vegetation module. CCSM3 is a global, coupled ocean–atmosphere–sea ice–land surface climate model without flux adjustment [*Collins et al.*, 2006]. The atmospheric model is the Community Atmospheric Model 3 (CAM3) with horizontal resolution of about 3.75°×3.75° and 26 vertical hybrid coordinate levels. The land model is the Community Land Model version 3 (CLM3) with the same resolution as the atmosphere. The ocean model is the NCAR implementation of the Parallel Ocean Program (POP) with vertical *z* coordinate with 25 levels. The longitudinal resolution is 3.6°, and the latitudinal resolution is variable, with finer resolution in the tropics. The sea ice model is the NCAR Community Sea Ice Model (CSIM). The resolution of CSIM is identical to that of POP. CCSM3 has previously been widely used in equilibrium and transient simulations of the glacial/interglacial climate state [*Shin et al.*, 2003a; *Otto-Bliesner et al.*, 2006; *Hu et al.*, 2007, 2008; *Liu et al.*, 2009; *Renold et al.*, 2009].

TraCE-21000 is the first try at representing the transient evolution of Earth's climate system over the last 21,000 years with the low-resolution version (T31_gx3v5) of CCSM3 [*Liu et al.*, 2009]. TraCE-21000 simulation includes two parallel runs DGL-A and DGL-B with different experimental schemes. Compared with DGL-B run, the DGL-A run more successfully represented global climate evolution according to reconstructed paleoclimate proxies (sea surface level, AMOC intensity, surface air temperature (SAT) in Antarctica and Greenland, and sea surface temperature (SST) in the tropical Atlantic Ocean) through a sudden termination of meltwater discharge into the North Atlantic at 14.67 ka. During the integration of the DGL-A run, external forcing such as meltwater discharge, insolation intensity, greenhouse gas (GHG) concentration, and land–ice sheet topography all varied in time based on reconstructed data [*Liu et al.*, 2009]. The key factor for the successful transient simulation is setting the scenario of meltwater discharge in high North Atlantic latitudes (50°–70°N) and the Gulf of Mexico from 19 to 14.67 ka. The total meltwater discharge is equivalent to a 50.1 m rising of the global sea level (the North Atlantic and Gulf of Mexico contribute 45.35 m and 4.75 m, respectively). The mean intensity of meltwater discharge is about 0.133 Sv. In the DGL-A run, AMOC is suppressed to a "turned off" state during Heinrich 1(H1) event (17 ka) with the increasing meltwater discharge into North Atlantic, and the "turned off"

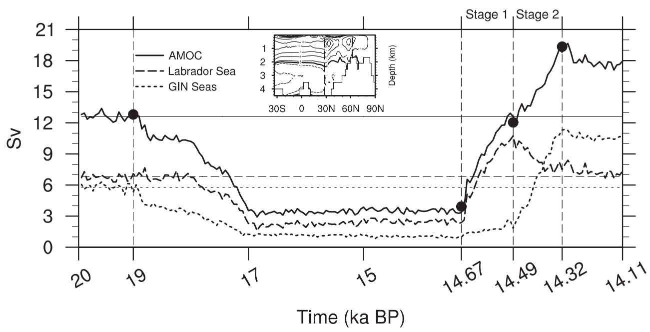

Figure 1. Two-stage feature of AMOC recovery (solid line) based on regional NADW formation volumes in the Labrador Sea (dashed line) and the GIN seas (dotted line) of model run DGL-A. AMOC intensity is defined as the maximum stream function of the Atlantic section below depths of 500 m. Regional NADW formation volume in the GIN seas is defined as the maximum stream function at its southern edge at 62°N. Regional NADW formation volume in the Labrador Sea is defined as the difference of AMOC intensity and regional volume in the GIN seas. Circles show the time of four climate states: the glacial state (GLA, 19 ka B.P.), pre-BA event (pre-BA, 14.67 ka B.P.), recovery (REC, 14.49 ka B.P.) and BA (14.32 ka B.P.). Horizontal dashed lines stand for the Last Glacial Maximum value of AMOC intensity and NADW formation volume in the Labrador Sea and GIN seas. Time periods of the two recovery stages are shown with "stage 1" (pre-BA–REC) and "stage 2" (REC-BA). Inset plot shows the latitude edges of each NADW region used to calculate regional NADW formation.

state of AMOC is maintained until the termination of meltwater discharge. In order to study the recovery process of AMOC from an initialized glacial state, we adapt the DGL-A run of TraCE-21000 simulation.

3. TWO-STAGE FEATURE OF AMOC RECOVERY

Inspired by the "alternative measuring method" of evaluating the AMOC, developed by *Gent* [2001], here we induce a new method to extract regional NADW formation volume in the Labrador Sea and GIN seas from the zonal mean stream function of the Atlantic. Regional NADW formation volume is calculated from the difference of vertical maximum stream function at the latitude edges of each NADW origin. Our method can present the individual volume of NADW formation in two origins quantificationally. The sum of NADW formation volume in two origins is equal to the value of AMOC intensity if we propose that AMOC intensity stand for the total NADW formation volume in the North Atlantic. Compared to the traditional method using maximum mixed

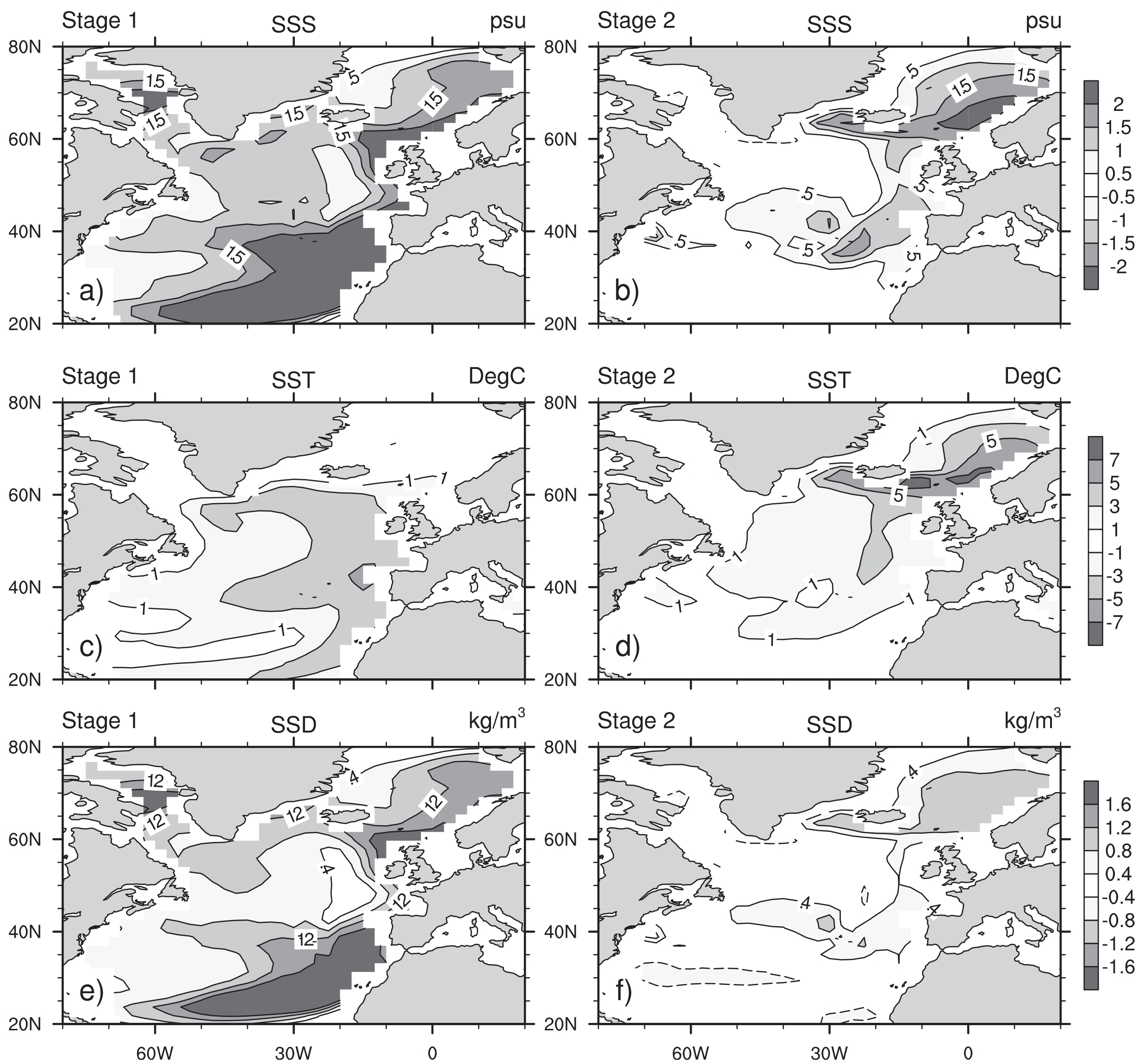

Figure 2. Change in (a and b) annual mean sea surface salinity (SSS), (c and d) sea surface temperature (SST), and (e and f) sea surface density (SSD) during (left) stage 1 and (right) stage 2. Solid and dashed contour lines indicate postive and negative values, respectively. Values of pre-BA/REC/BA are all presented with ±10 year means here and in Figures 3–5.

layer depths [*Renold et al.*, 2009] or area mean vertical velocity [*Vellinga and Wood*, 2002], this method is one alternative way to precisely quantify the NADW formation volume and to detect variation of the regional volume of NADW formation in its multiple origins.

A two-stage feature of AMOC recovery is revealed in this regional analysis of NADW formation during the AMOC recovery period (BA onset), based on the asynchronous reinitiation of NADW in the Labrador Sea and GIN seas (Figure 1). After meltwater discharge in the North Atlantic, NADW formation in the Labrador Sea and GIN seas is suppressed to nearly a “turned off” state after the H1 event, the state in which nearly no NADW was formed. After that, during the recovery period of the AMOC (starting from 14.67 ka), NADW formation first reinitiates in the Labrador Sea, defined here as stage 1 of AMOC recovery (from pre-BA to REC), and subsequently reinitiates in the GIN seas, which constitutes stage 2 (from REC to BA).

During stage 1, once the meltwater forcing in the North Atlantic is suddenly halted, NADW formation in the Labrador

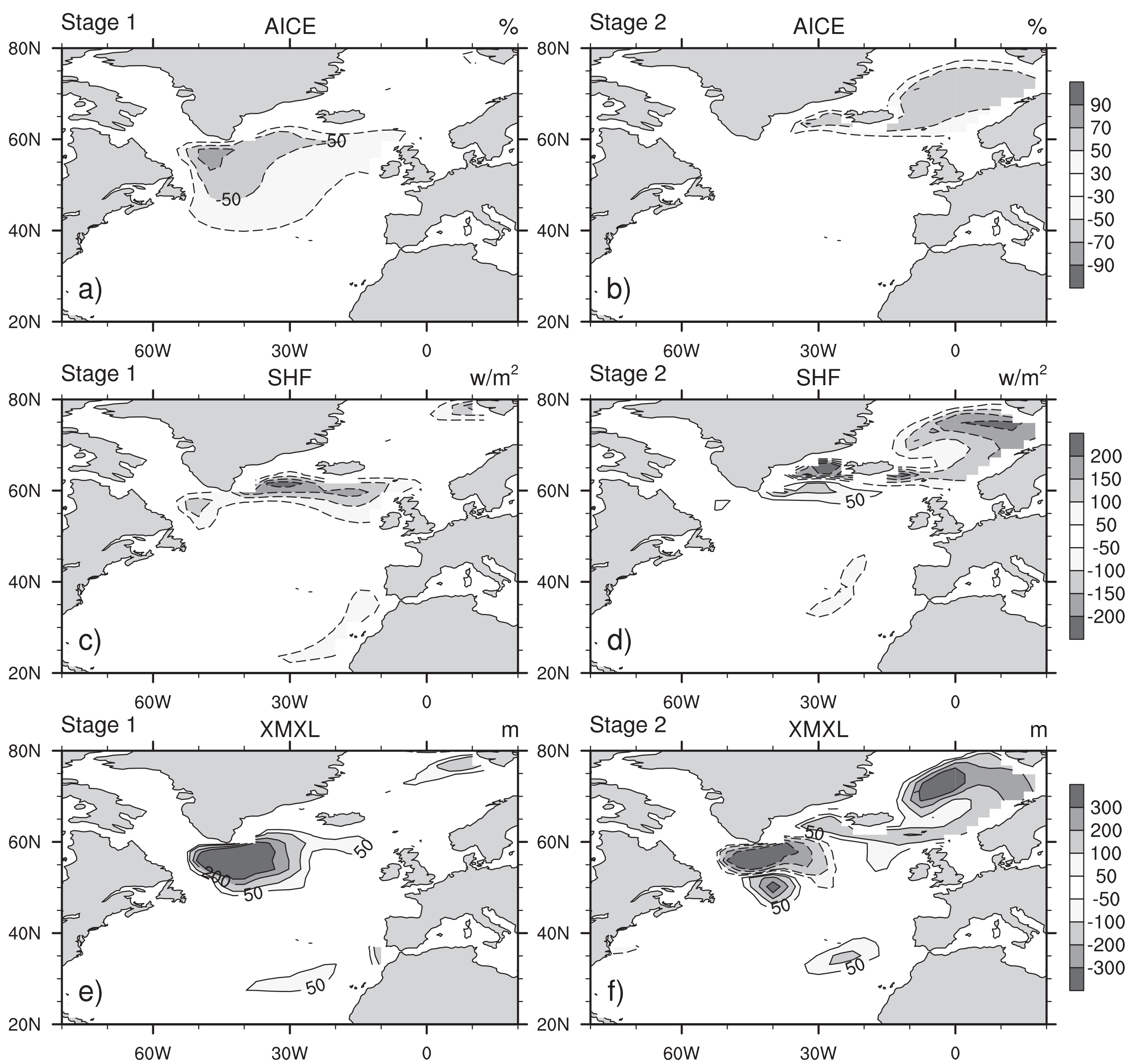

Figure 3. Change in (a and b) annual mean sea ice concentration (AICE), (c and d) surface heat flux (SHF), and (e and f) maximum mixed layer depth (XMXL) during (left) stage 1 and (right) stage 2. SHF is downward; negative value means oceanic heat loss.

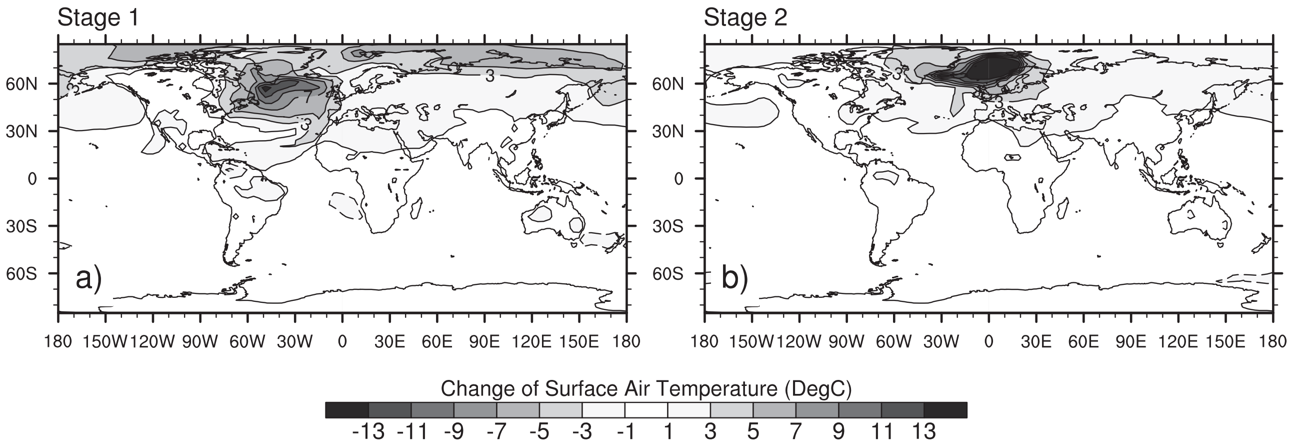

Figure 4. Change in annual mean surface air temperature (SAT) during (a) stage 1 and (b) stage 2. Units are in degrees Celsius (°C).

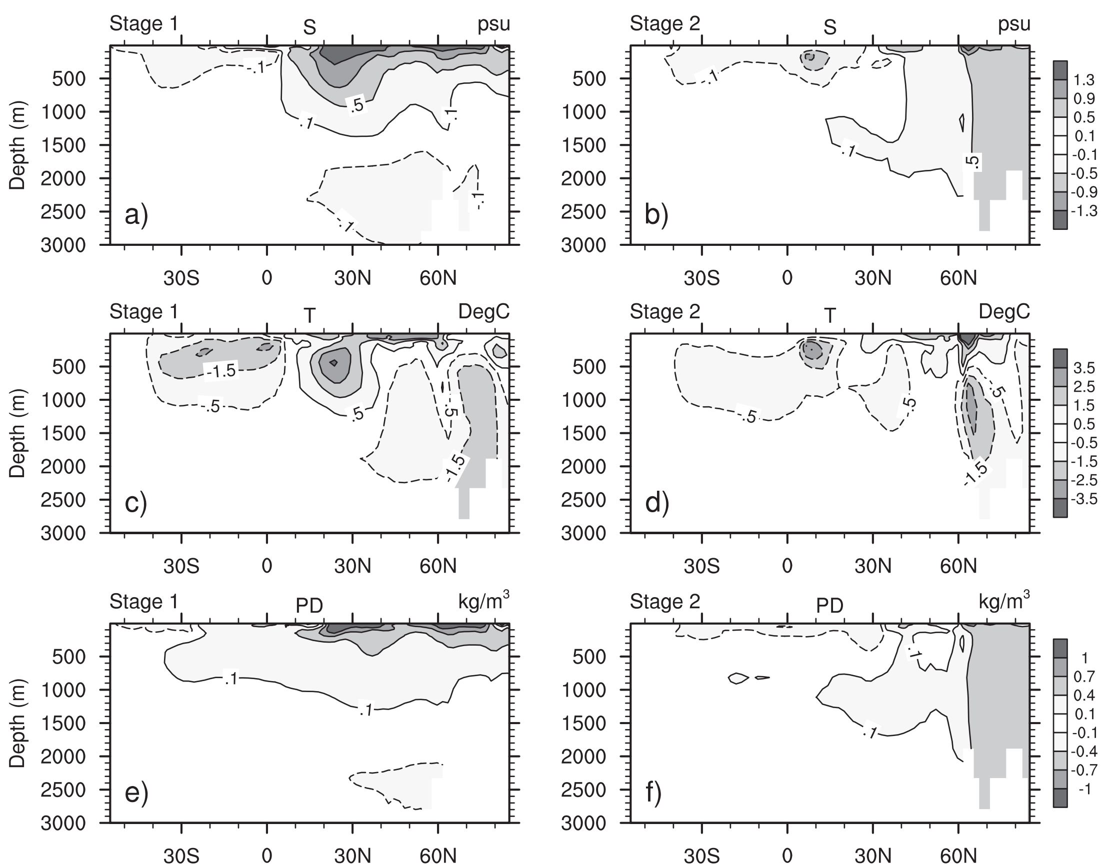

Figure 5. Change in (top) annual mean salinity (S), (middle) potential temperature (T), and (bottom) potential density (PD) during (left) stage 1 and (right) stage 2 in the zonal averaged Atlantic section.

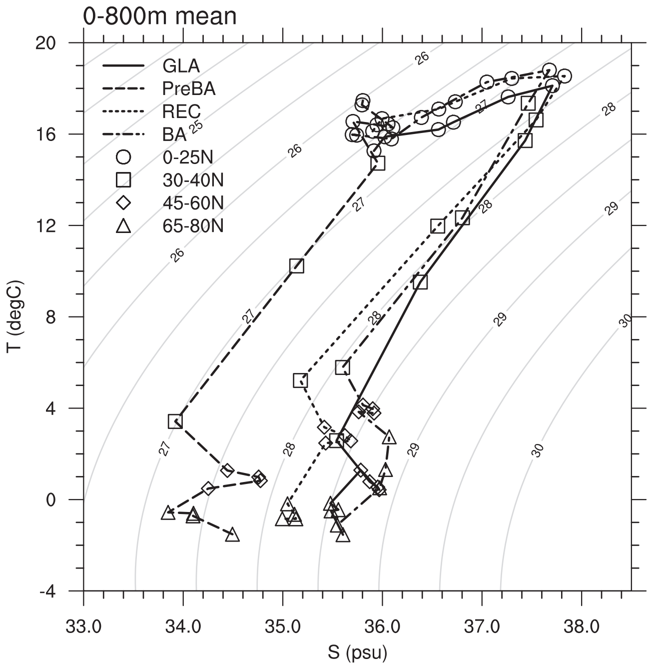

Figure 6. T-S diagram of the North Atlantic upper layer water (0–800 m) for GLA (solid line, mean within 20–19 ka), pre-BA (dashed line, 14.67 ka), REC (dotted line, 14.5 ka) and BA (dash-dotted line, 14.32 ka). Latitude bands are shown with different markers (circle for the tropical North Atlantic, square for the subtropical North Atlantic, diamond for the subpolar North Atlantic which includes the Labrador Sea, and triangle for the GIN seas). Latitude interval is 5°.

Sea is activated from the "turned off" state to the enhanced state (above initialized volumes) within 150 years. This has the result that while NADW formation in the GIN seas has not fully recovered by the end of stage 1, the total volume of NADW formation in the North Atlantic (AMOC intensity) reaches its original glacial level at the end of stage 1 (REC). Thereafter, the continuing recovery of NADW formation in the GIN seas in stage 2 pushes the AMOC intensity to an even higher level (about 20 Sv) within 170 years. Continuous increasing of AMOC intensity results in a robust AMOC overshoot phenomenon on a time scale of hundreds of years and a mean state transition of AMOC from 12.5 Sv at the Last Glacial Maximum to about 17.5 Sv at interglacial state (stable AMOC intensity during BA, similar to its modern simulated value of about 17 Sv in CCSM3 according to *Renold et al.* [2009]). On the basis of the precondition from stage 1, it is evident that the rapid recovery and subsequent overshoot of the AMOC can largely be attributed to the speed and magnitude of enhanced NADW formation in the GIN seas during stage 2.

The two-stage feature of AMOC recovery can also be confirmed by changes in associated sea surface variables in the Atlantic Basin (Figures 2 and 3), surface air temperature (SAT) (Figure 4), and zonal mean salinity, temperature, and potential density (Figure 5).

As shown in Figure 2, sea surface salinity (SSS) and sea surface density (SSD) of the whole North Atlantic Basin and SST of south of Greenland significantly increase during stage 1. However, during stage 2 the increase in SSS, SST, and SSD primarily happens in the GIN seas. SSS and SSD do increase somewhat in the GIN seas during stage 1 but not enough to induce robust NADW formation, as shown in Figure 1. The reason why the increased SSS and SSD in the GIN seas during stage 1 did not induce the robust reinitiation of NADW will be addressed in section 4.

The changes in sea ice cover (annual mean sea ice concentration), surface heat flux (SHF) (downward) and maximum mixed layer depths provide a clearer picture of the two-stage feature in the Labrador Sea and GIN seas (Figure 3). Because of the coarse resolution of the model used here and other similar models, the simulated deepwater formation regions are broader than the Labrador Sea and GIN seas. For simple presentation, here we refer to them as the Labrador Sea and GIN seas to present the surrounding changes in general. The Irminger Sea also has similar significant changes to the GIN seas during stage 2. Because of its small area and complex structure (shown in Figure 3), here and in following sections

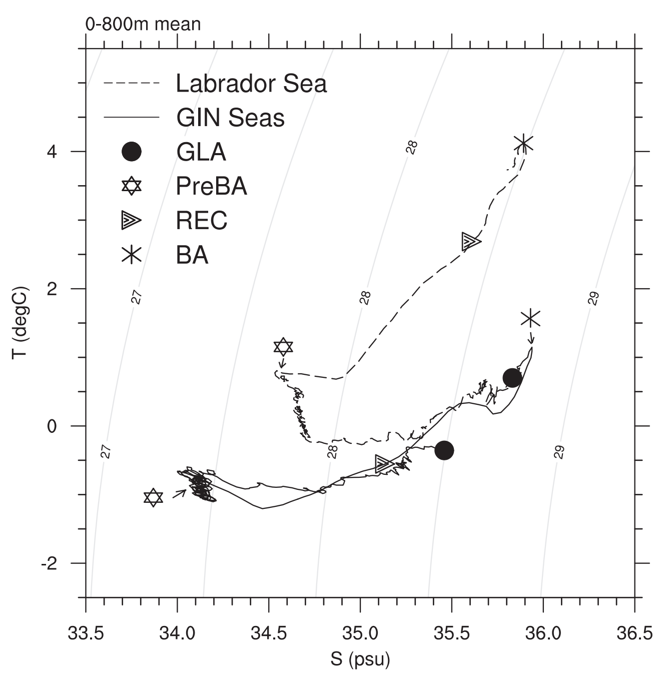

Figure 7. T-S diagram of the Labrador Sea (dashed line, 50°–62°N) and GIN seas (solid line, 62°–80°N) within upper layers (0–800 m). GLA/pre-BA/REC/BA are shown with different symbols.

the Irminger Sea is included with the GIN seas to avoid a too complex discussion. Changes in these three variables are seen primarily around the Labrador Sea during stage 1 and around the GIN seas during stage 2. It is clear that sea ice cover is tightly connected with the increasing SST (Figure 2) in both NADW origins and similarly with oceanic heat loss and convection.

In Figure 4, SAT increases within nearly the whole Northern Hemisphere during stage 1, with a maximum about 15°C around the Labrador Sea during stage 1, and then the warming center moves to the GIN seas during stage 2.

In Figure 5, we see that the zonal mean salinity/temperature/potential density of the whole Atlantic Basin exhibits a simultaneous shift, with salinization/warming/densification of upper layers and the opposite change in deeper layers. This primarily happens in the Labrador Sea during stage 1 and then moves to the GIN seas during stage 2. An exception to these simultaneous shifts in ocean conditions is the subtropical North Atlantic, where Ekman pumping becomes a significant factor. Ekman pumping drives the recovered northward warm and salty water of upper layers to the depth of about 500 m, that is why the maximum change of salinity and temperature at the depth of 500 m in Figure 5, also for the SSS and SSD change in Figure 2, occurs during stage 1 in the subtropical North Atlantic. A more detailed discussion of salinity/temperature/potential density evolution within the two main NADW origins will be the topic of the following section.

The two-stage feature of AMOC recovery becomes apparent through an analysis of NADW formation by region, and it is confirmed by the associated ocean and atmosphere variables. Even though the overall evolution of AMOC intensity lacks an obvious two-stage feature, our regional analysis shows that a two-stage feature exists in the simulated recovery process of AMOC during the last deglaciation.

4. CAUSES OF TWO-STAGE AMOC RECOVERY

The preceding analysis suggests the two-stage evolution of AMOC recovery depends on the asynchronous reinitiation of NADW in the Labrador and GIN seas, but we have yet to determine the reasons for this asynchronicity. In this section, we present the time evolution of salinity/temperature/potential density, give a detailed account of deepwater formation

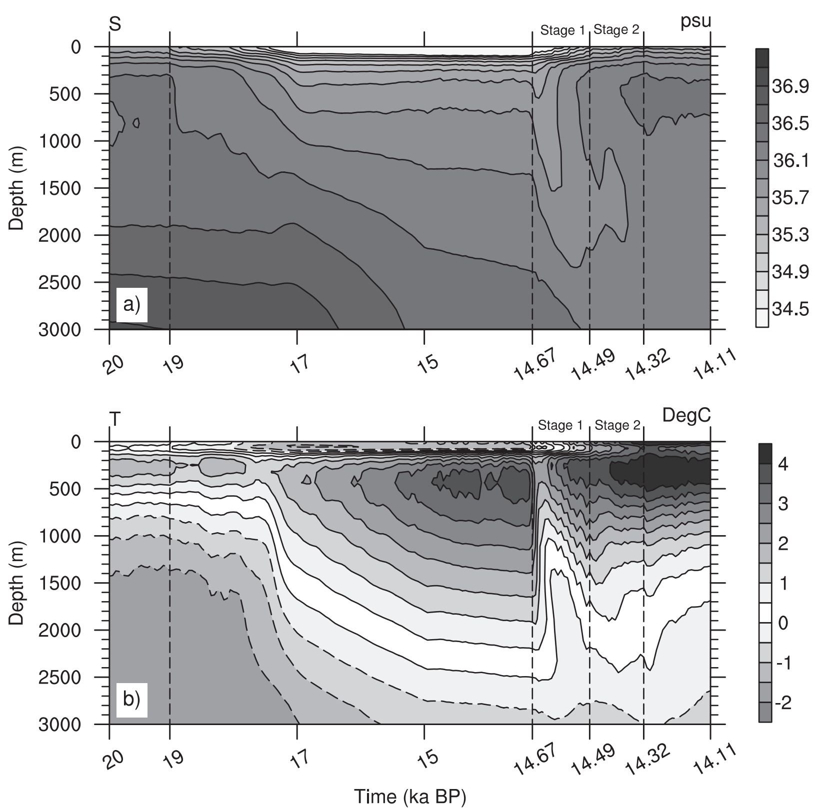

Figure 8. Hovmöller diagram of (a) annual mean salinity (S) and (b) temperature (T) in the Labrador Sea, averaged between 50°N and 62°N.

in each region, reconsider the mechanisms controlling NADW reinitiation, and finally, discuss the role of each NADW formation region in the simulated AMOC recovery and overshoot.

4.1. Evolution of Salinity/Temperature/Potential Density

Figure 6 shows the temperature-salinity (T-S) diagram of North Atlantic upper layers (0–800 m) at GLA, pre-BA, REC, and BA. Generally, the northward increase of potential density within upper ocean layers is controlled more by the temperature gradient than salinity north of 30°N. However, comparing the four consecutive ocean states, the change of potential density during meltwater discharge (GLA to pre-BA) and recovery periods (pre-BA to REC in the Labrador Sea and REC to BA in the GIN seas) is mainly controlled by salinity. During stage 1 (black line to light shaded line), salinity and potential density in the whole North Atlantic (excluding the tropical region) significantly increase, especially for the subtropical North Atlantic. During stage 2 (light shaded line to medium shaded line), salinity and potential density changes mainly happen in the GIN seas. Usually, an increase in salinity is accompanied by warming, but here it is clear that densification of North Atlantic upper layers is controlled more by salinity than temperature. Figure 7 provides another more detailed T-S evolution of upper layers in the Labrador Sea and GIN seas to support the salinity control over potential density change. During the periods of meltwater discharge and recovery, the changes of salinity, both for the Labrador Sea and GIN seas, not only contribute to the change of potential density but also compensate the opposite effect of temperature.

A Hovmöller diagram of area mean salinity and temperature in the Labrador Sea (Figure 8) shows that during the meltwater discharge period (from 19 to 14.67 ka), the Labrador Sea was freshened in all depths, with significant subsurface warming. The warming and freshening signal is mostly inhibited in upper layers (about 0–800 m) through suppressed convection, while turbulent mixing slowly spread the freshening and warming subsurface water to deeper layers. When meltwater discharge is terminated at 14.67 ka, convection in the Labrador Sea is quickly reinitiated, characterized by the sharp downward penetration of freshened water and the release of stored subsurface heat. The depth affected by the

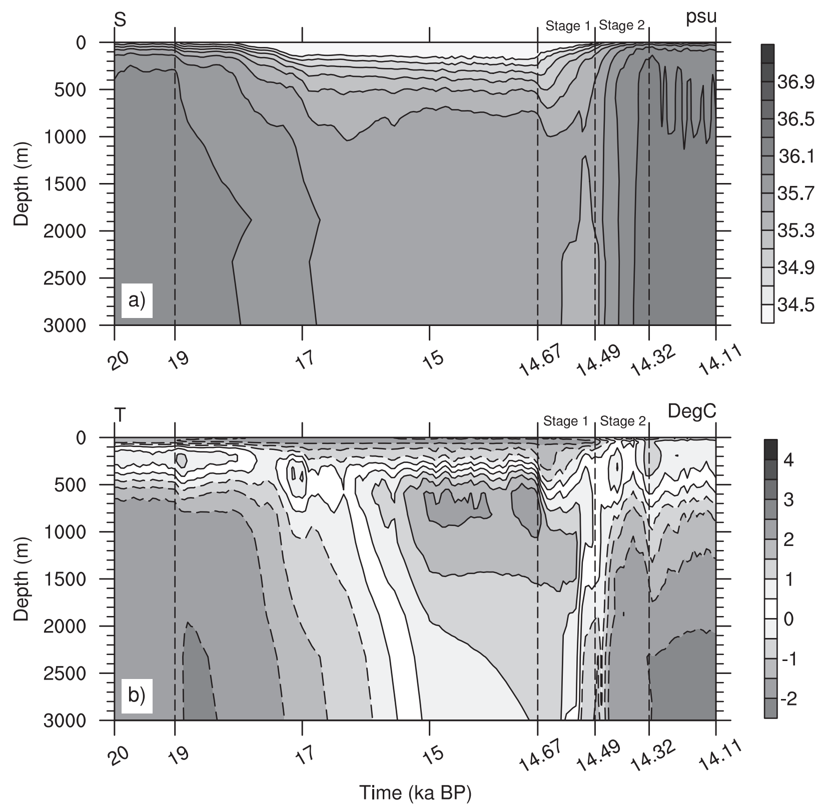

Figure 9. Hovmöller diagram of (a) annual mean salinity (S) and (b) temperature (T) in the GIN seas, averaged between 62°N and 80°N.

reinitiation of convection is limited to the approximately upper 2000 m. After the first sign of convection reinitiation, salinity and temperature both increase noticeably in the upper 2000 m, as a result of the resumed upper layer salt/heat transport from lower latitudes. The deep warm/fresh anomalies in the Labrador Sea soon dissipate, so that the change of salinity and temperature in Labrador Sea mainly happens during stage 1.

Similar to the Labrador Sea, a Hovmöller diagram of area mean salinity and temperature in the GIN seas (Figure 9) shows that the whole depth recovery of salinity and release of stored subsurface heat mainly occurs during stage 2. During stage 1, freshened water in the GIN seas penetrates downward several hundred meters, accompanied by the release of stored subsurface heat within several hundred meters too. However, the dynamic environment during stage 1 is still not sufficient to reinitiate the convection to deeper depths in this region and delays the reinitiation of NADW formation in the GIN seas to stage 2. During stage 2, salinity quickly increases at all depths, ultimately reaching higher levels than the initial glacial state (Figure 9a) and is accompanied by subsurface heat release with warming in the upper layers and cooling in the deeper layers (Figure 9b).

The evolution of potential density at depth in the Labrador Sea and GIN seas confirms the main conclusions from the Hovmöller diagram of salinity and temperature in these two regions (Figure 10). The increasing of potential density in Labrador Sea mainly happens during stage 1 within the upper 1000 m and in the GIN seas during stage 2 within the entire water column. A key development occurs in the GIN seas during stage 1, where a very weak stratification is formed followed by the densification of the entire water column at the onset of stage 2. It is derived by the increasing of the upper layers potential density and the small change in the deep layers. This extremely weak stratification provides a background for subsequent strengthened reinitiation of convection and NADW formation in the GIN seas during stage 2. The physical process of extremely weak stratification and reinitiation of NADW in the GIN seas is similar to the “density threshold” described by *Krebs and Timmermann* [2007a, 2007b] and *Renold et al.* [2009]. Now we will present the physical process in more detail.

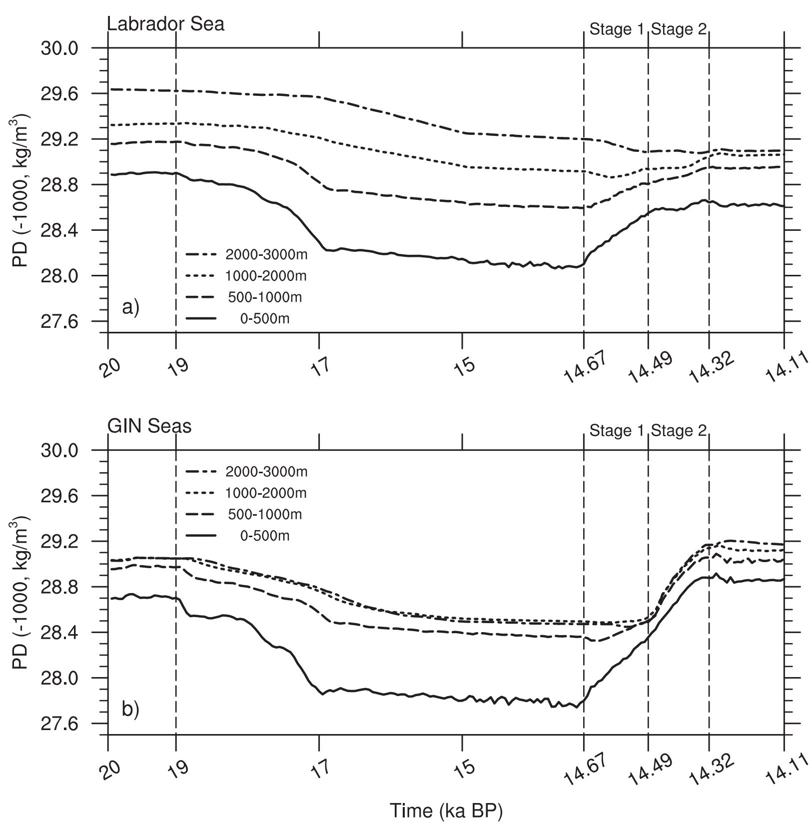

Figure 10. Annual mean potential density (PD) of the (a) Labrador Sea (50°–62°N, 70°–45°W) and (b) GIN seas (62°–80°N, 45°W–20°E), separated into vertical ocean layers.

4.2. Reinitiation of NADW Formation

The general picture of NADW formation in multiple origins from an unperturbed state could be described as follows: through air-sea heat and freshwater exchange, salty and warm water is transported to the North Atlantic within the upper ocean layers, which are driven by a meridional steric gradient; fresh and cold water sinks downward through deep convection in both NADW origin regions, i.e., Labrador Sea and GIN seas, and then moves southward driven by a deep ocean meridional pressure gradient.

As shown above, the recovery of AMOC is accompanied by increasing salinity (shown in Figures 6–9) and the retreat of sea ice cover (Figure 3) in the North Atlantic. The change in salinity is due to net salinity advection from low latitudes within the upper layers, and the retreat of sea ice cover significantly affects the local heat–freshwater exchange in the NADW origins. It seems natural that the evolution of these two processes should play a significant role during the AMOC recovery period. On the basis of this preliminary understanding of NADW formation processes, we investigate the simulated NADW reinitiation process during the AMOC recovery period of the last deglaciation.

The net salt transport to the Labrador Sea decreases during meltwater discharge, and it resumes primarily during stage 1 (Figure 11a), consistent with the increase in salinity in this region (Figure 8a). Before stage 1, the water of the Labrador Sea in its entire depth is significantly freshened and lightened through thousands of years of freshwater discharge. During stage 1, the transport of salty and dense water in upper layers into this area (Figures 8a and 10a) could directly induce a reversed vertical density structure (Figure 8a). The reversed density structure is followed by a resumed convection. As convection reinitiates, the net heat transport into the upper layers also increases (Figure 11b). This heat transport comes from both stored subsurface heat release (Figure 8b) and resumed warm water advection from low latitudes. This induces the abrupt retreat of sea ice in the Labrador Sea (Figure 12a) and a corresponding increase in surface heat loss (seen as a decrease in SHF) (Figure 12b).

The local oceanic surface heat loss and nonlocal salt water advection to the Labrador Sea in the upper ocean layers combine to cause upper layer densification, (Figure 10a) and thus the abrupt resumption of convection (Figure 12c). Subsurface warming also contributes to the resumption of convection, favoring a reversed vertical density structure. However, the subsequent convection quickly induces the subsurface heat anomaly to dissipate as it is ventilated (Figure 8b). These three factors simultaneously force NADW formation in the Labrador Sea to an enhanced level beyond its initial intensity (Figure 1, black line).

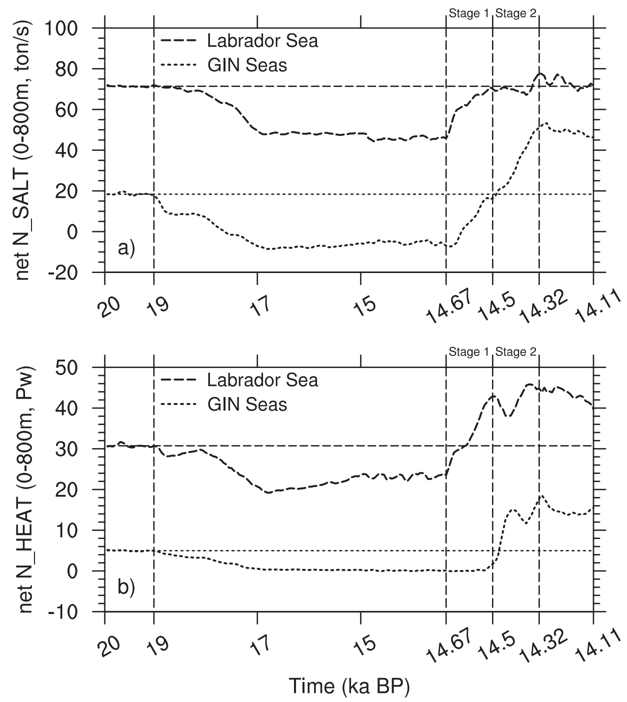

Figure 11. Net (a) salt and (b) heat transport in upper layers (0–800 m) for the Labrador Sea at 50°–62°N, dashed line, and GIN seas, 62°–80°N, dotted line.

The resumption of convection in the Labrador Sea spreads the dense water to nearly its whole depth and induces a meridional steric difference in the surface (Figure 13a, black line) and pressure difference in the deep ocean between the Labrador Sea and its southern ocean (Figure 13b, black line). This further induces resumption of northward salt/heat advection within the upper layers from low latitudes to the Labrador Sea (Figure 11) and southward deepwater flow from the Labrador Sea to low latitudes (Figure 1).

In the GIN seas, the reinitiation process of NADW formation during stage 2 is similar to the Labrador Sea, except the GIN seas first undergo a preconditioning process during stage 1. Net salt transport to the GIN seas within the upper layers resumes during stage 1 (Figure 11a), but net heat transport in the upper layers remains suppressed during this stage (Figure 11b). The net salt transport to the GIN seas induces the densification of its upper layers (Figures 2e and 10b), which causes shallow reinitiation of convection during this stage (Figure 12c) and is characterized by shallow penetration of freshened water and stored subsurface heat release (Figure 9). However, at this time, the dynamical environment is still not sufficient to reinitiate strong deep convection (Figures 9 and 12c) and NADW formation (Figure 1). The resumption of net heat transport to the GIN seas in the upper

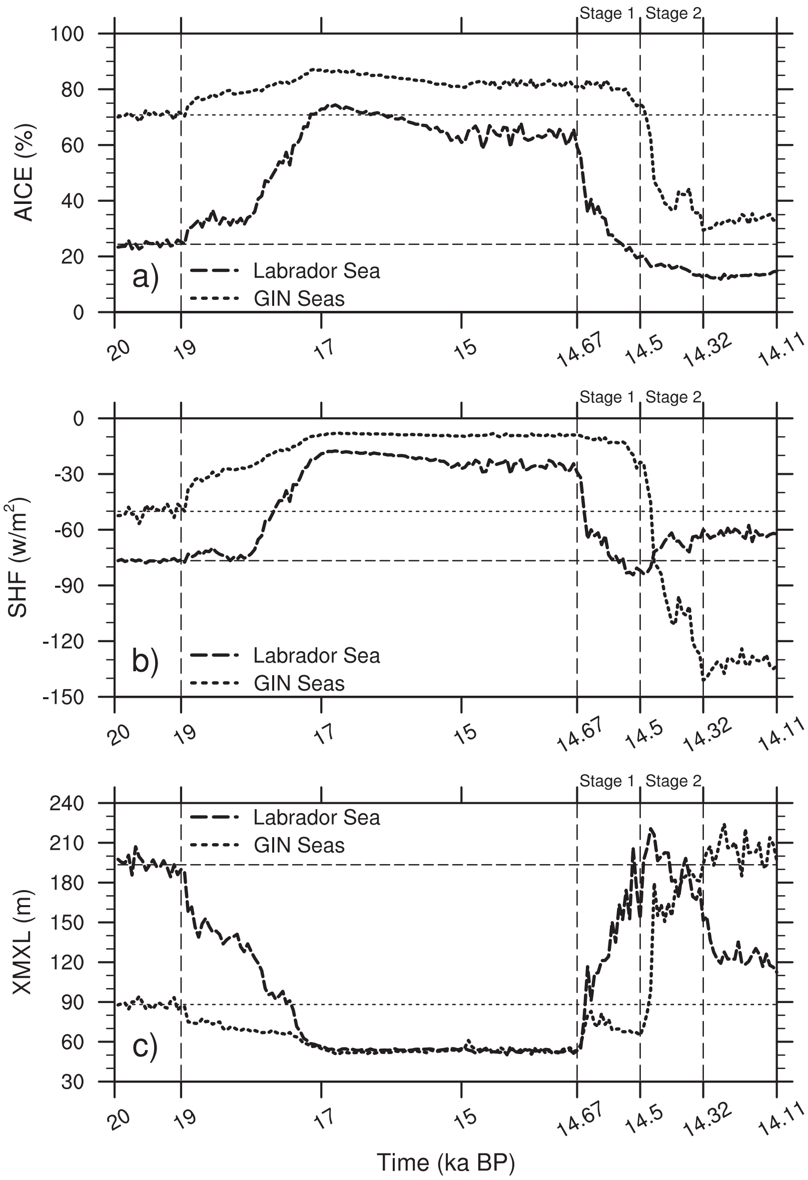

Figure 12. (a) Annual mean sea ice concentration (AICE), (b) surface heat flux (SHF), and (c) maximum mixed layer depth (XMXL). Dashed and dotted lines represent regional mean values for the Labrador Sea and GIN seas, respectively.

layers during stage 2 (Figure 9b) induces sea ice retreat (Figure 12a) and an abrupt shift in SHF (Figure 12b). Only after that, do deep convection (Figure 12c) and NADW formation (Figure 1) resume in the GIN seas. Meanwhile, the GIN seas steric and deep-pressure difference resume a little during stage 1 and then more robustly during stage 2 (Figure 13, shaded line). During stage 2, the relevant variables in the GIN seas can be seen to undergo an extreme shift and are enhanced above initial glacial values by a factor of 2 or more in many cases (Figures 11–13, shaded line). All These changes cause a strong reinitiation of NADW formation (Figure 1, light shaded line) and saltier/denser water in the GIN seas (Figures 9a and 10b). The denser water in the GIN seas at end of stage 2 contributes to the persistence of the AMOC overshoot and the mean state transition of AMOC (Figure 1, black line).

Among three factors, which promote NADW formation in the Labrador Sea and GIN seas, contributions of two factors significantly decrease or disappear at the end of each stage. One is the contribution of salinity advection, which is based on the salinity difference between the advected salty water

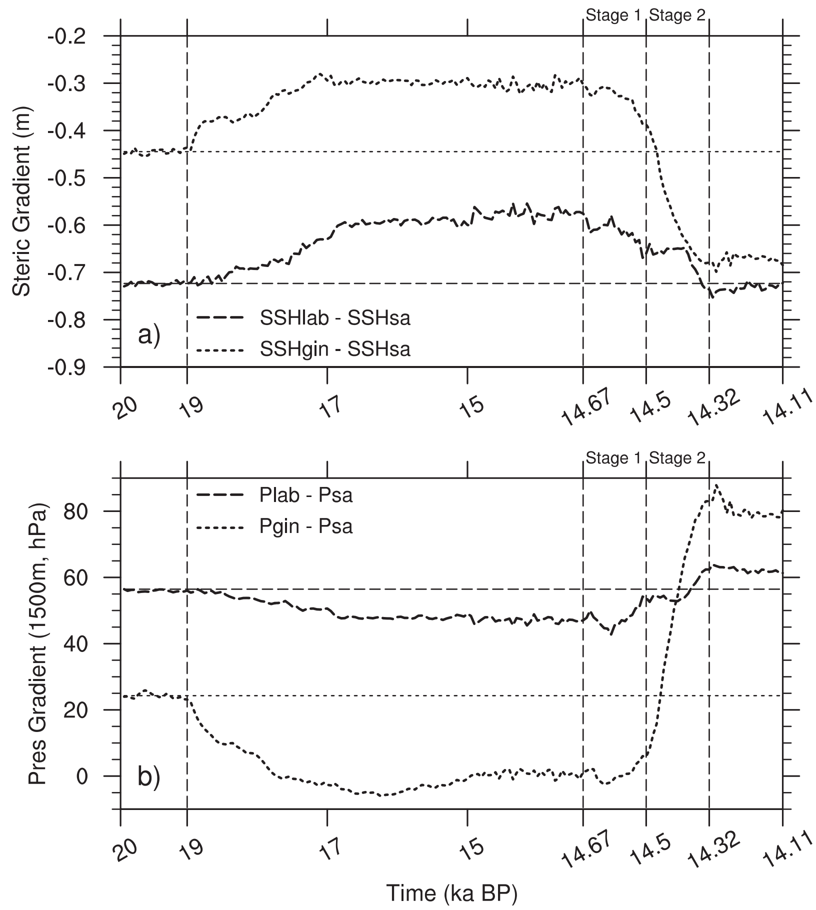

Figure 13. (a) Southward steric gradient (SSH_{lab}, 50°–62°N; SSH_{gin}, 62°–80°N; and SSH_{sa}, 30°S–50°N) and (b) deep ocean pressure gradient (1500 m, hPa) of the Atlantic Basin. Dashed and dotted lines represent values from the Labrador Sea and GIN seas, respectively.

and the local freshened water in the deeper layers of two regions of origin (Figure 14). Another is the contribution of subsurface warming, which disappears when convection is restarted (Figures 8b and 9b). These two processes together induce enhanced NADW formation in each NADW region, and their effects subside at the end of each corresponding stage (Figure 1).

According to the above analysis, contributions of salinity dominate the change of potential density in both NADW regions (Figure 7), and the subsurface heat anomaly provides an additional reversed vertical density structure for convection reinitiation in both stages (Figures 8b and 9b). The main contribution of net heat transport within the upper layers is to melt extended sea ice cover during each stage, which is shown to be of crucial importance in the reinitiation of deep convection in both NADW regions of origin (Figures 11b and 12c).

4.3. A Reconsidered Mechanism for NADW Reinitiation

On the basis of the comprehensive analysis of variables relevant to NADW formation in the DGL-A run, and the previous hypothesized mechanisms [*Vellinga and Wood*, 2002; *Yin et al.* 2006; *Krebs and Timmermann*, 2007a, 2007b], here we reconsider the mechanisms controlling NADW reinitiation with some clarified details (Figure 15).

In our reconsidered mechanism, we identify two dominant processes affecting NADW reinitiation. The first one is the local process as shown in Figure 15 (box 1 to box 2 to box 3 to box 4 to box 5 to box 6 to box 7 to box 1). This process is mainly dominated by the resumption of surface density flux over NADW origins. Resumption of surface density flux, primarily controlled locally by the retreat in sea ice cover, is largely initiated by northward heat transport to NADW formation regions (Figures 11b and 12a), then densified NADW

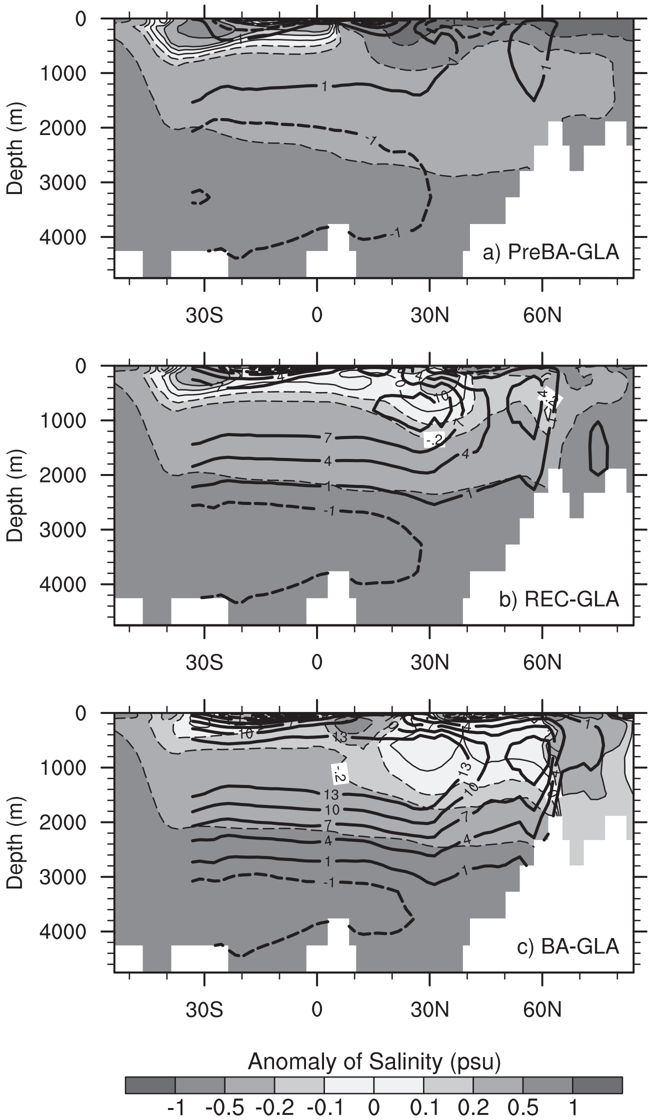

Figure 14. Change in Atlantic zonal averaged salinity anomaly (shading with thin contours) and AMOC stream function (thick contours) during (a) pre-BA–GLA, (b) REC-GLA, and (c) BA-GLA.

origin's surface layer reduces the stratification and starts the reinitiation of NADW. Here we can use SHF as a representation of surface density flux because its contribution to the density flux is dominant [*Shin et al.*, 2003b]. Second is the nonlocal process shown in Figure 15 (box 1 to box 4 to box 5 to box 6 to box 7 to box 1). The salty/dense water transport into the upper layers of each region (Figures 11a and 14) overlies fresher and lighter local water in deeper layers (Figure 14), directly reduces the stratification, and starts the reinitiation of NADW. The local deepwater formation from surface density flux and nonlocal dense water transport simultaneously contributes to the total NADW reinitiation during the whole recovery period.

This reconsidered mechanism provides a clearer picture of how NADW reinitiation could occur after meltwater discharge in the North Atlantic, with some important details that were lacking in previous proposed mechanisms such as the nonlocal process [*Vellinga and Wood*, 2002; *Yin et al.*, 2006; *Krebs and Timmermann*, 2007a, 2007b]. The contribution of subsurface warming to the reinitiation of NADW is not found to be a significant positive feedback, it is seen as a trigger for NADW reinitiation because of its effect on sea ice cover in each region, so we find that the other two processes are the factors responsible for the two-stage feature of AMOC recovery in this reconsidered mechanism.

4.4. Nature of Two-Stage Feature

As shown above, the reinitiation process of NADW formation in two main regions of origin is robustly asynchronous, first in the Labrador Sea and then in the GIN seas. So far, the cause of this asynchronous feature is still a critical issue for the understanding of AMOC recovery.

First, we should notice the difference between the NADW formation under an unperturbed background state and the recovery state after the halting of meltwater discharge. The variation of NADW formation during an unperturbed state is dependent on the local ocean surface density flux. However, during the period of recovery, there is a large-scale retreat of extended sea ice cover that directly affects the surface density flux and allows NADW reinitiation to occur. Another difference with the unperturbed state is that during the AMOC recovery period, the North Atlantic is freshened at greater depths than in other oceans, and the AMOC recovery process is accompanied by the resumption of salinity advection in the North Atlantic in the upper layers, enhancing NADW formation directly. So, owing to the unique local and nonlocal processes affecting NADW formation during AMOC recovery, the dynamical ocean environment is very different from the unperturbed state.

Second, two kinds of processes, which are mentioned in the reconsidered mechanism, each induce the asynchronous feature of the NADW reinitiation in its two origins. As discussed above, the local process is mainly affected by the extended sea ice cover, which retreats primarily as a result of heat transport from low latitudes. Since the GIN seas are located northward of the Labrador Sea, the sea ice retreat happens in the Labrador Sea before the GIN seas.

Third, it was also found that the efficiency of the nonlocal dense water transport is mainly controlled by the intensity of advection within the upper layers and meridional salinity gradient (Figure 14). After the freshening of the North

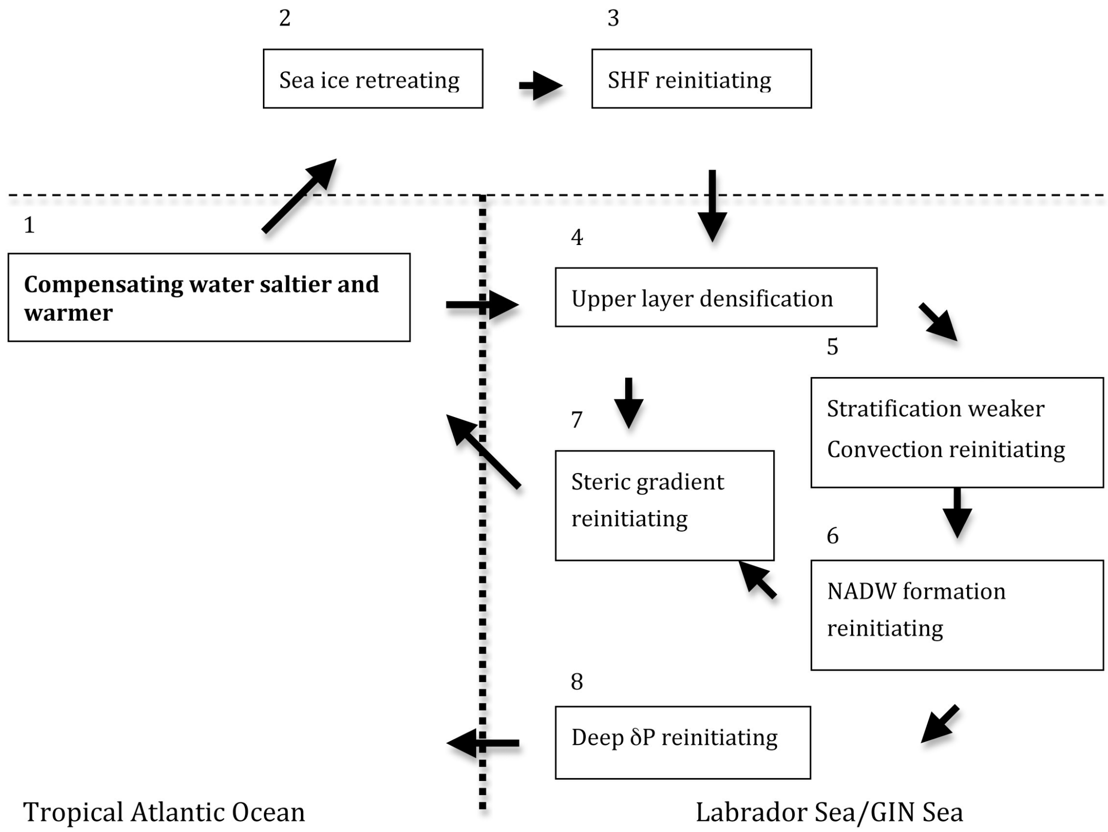

Figure 15. Schematic illustration of the proposed positive feedback process controlling reinitiation of NADW formation in Labrador Sea and GIN seas. Meridional pressure difference is indicated by δP.

Atlantic from meltwater discharge, the whole North Atlantic Basin is nearly homogeneous for salinity, so the salinity gradient at the south boundary of NADW regions is important for salt transport. During the AMOC recovery period, the maximum meridional salinity gradient within the upper layers of the North Atlantic moves northward.

On the basis of our reconsidered mechanism of NADW reinitiation, only after NADW formation is fully reinitiated in the Labrador Sea, does the dynamical environment of the GIN seas result in full convective reinitiation. So the combination of local and nonlocal mechanisms causes NADW formation reinitiation in the Labrador Sea and GIN seas to be asynchronous, and the sequence of reinitiation is northward.

5. DISCUSSIONS AND CONCLUSIONS

In this analysis, we found that the simulated AMOC recovery during the last deglaciation occurred in two stages: first, in the Labrador Sea and then in the GIN seas. We described how the two-stage feature of AMOC recovery depends on the asynchronous reinitiation of NADW formation in the two regions of origin with a reconsidered mechanism. We also suggest that the two-stage feature of AMOC recovery should not just depend on the evolutionary characteristics of a time series of AMOC intensity because a single time series is not sufficient to present the reinitiation process of NADW formation in multiple origins, synchronous or otherwise. Comparing the results of *Renold et al.* [2009], our results provide more physical and geographical analysis with the same model CCSM3 by providing a clearer and more complete mechanism, and these results are doubly interesting because they are based on a particular historical event of abrupt climate change.

Our results, in addition to previous work such as that of *Vellinga and Wood* [2002] and *Renold et al.* [2009], point out that the Labrador Sea and GIN seas both provide a comparable robust contribution to the AMOC recovery. However, some recent work also shows that the role of the multiple origins of NADW formation in AMOC variability and stability, as derived from different models [*Bentsen et al.*, 2004; *Mignot and Frankignoul*, 2005; *Latif et al.*, 2006; *Spence et al.*, 2008], is uncertain. Despite the dependence of model, however, the time scale should not be ignored when addressing the relative contribution of NADW multiple origins to AMOC change. For a time scale of interdecades or shorter in control simulation, the conclusions about the relative contribution do not seem consistent; but for a centuries or longer time scale in water-hosing experiments, the conclusions are consistent because of the big perturbation and large response according to current literature.

In this chapter, we use one new method, which is based on the zonal mean stream function of the Atlantic, to present the two-stage feature of the AMOC recovery in multiple regions of origin of NADW formation primarily. However, the two-stage feature not only depends on the new method but must also be confirmed in the traditional way, through examination of the mixed layer depth in Figure 12c and other different variables (Figures 2–5 and 8–13). The new method is not only capable of representing the change of NADW formation in multiple origins, it can quantify the volume of NADW formation in multiple origins, which cannot be achieved through the traditional way.

The results of the DGL-A run are consistent with an idealized water-hosing experiment under the Last Glacial Maximum state (not shown here). In this idealized water-hosing experiment, AMOC intensity fully recovered by the end of integration (1500 years). In this idealized experiment, stage 2 of AMOC recovery is mainly dominated by the adjustment process of NADW formation in the GIN seas with a time scale of about 500 years. The difference between these two simulations in the recovery of AMOC is that the AMOC intensity of DGL-A jumped to interglacial levels during the recovery process, forced by increased GHG concentration and orbital insolation [*Liu et al.*, 2009]. This difference is not critical to our dynamical analysis of the AMOC recovery process.

In considering the recovery process of the AMOC during last deglaciation, the AMOC overshoot is important in the generation of BA warming in TraCE-21000. So the AMOC overshoot phenomenon may be critical to the understanding of abrupt climate change. As shown above, the development of the AMOC overshoot depends on enhanced NADW formation in the GIN seas during stage 2. Another important aspect of AMOC recovery in DGL-A is the mean state transition of the AMOC from a glacial to an interglacial state. This transition depends significantly on the intensified NADW formation in the GIN seas during BA onset as well. So the GIN seas are not only a key region for the development of an AMOC overshoot but also the key region for mean state transition of AMOC within glacial/interglacial cycles.

With our interpretation of the asynchronous reinitiation of NADW in the Labrador Sea and GIN seas, we speculate that the southward order of NADW reinitiation from the GIN seas to the Labrador Sea by *Vellinga and Wood* [2002] may be caused by an absence of a shift in sea ice cover during periods of "artificially" suppressed AMOC, so the sequence of reinitiation of convection in multiple regions in the Vellinga and Wood work may not be correct. The conclusions of *Renold et al.* [2009] are reasonably correct for their experiments with a "real" AMOC suppressing process. Beyond our results, one point should be mentioned: the contrast reinitiation sequence of NADW is based on two models, northward sequence by *Renold et al.* [2009] and our study from CCSM3 and southward sequence by *Vellinga and Wood* [2002] from HadCM3. Despite the dependence of the experimental scheme we mentioned before, the sequence of NADW reinitiation may also be dependent on models, but this needs further validation.

In our DGL-A model run, the time delay between the onset of stage 1 and stage 2 generally coincides with the recovery of the AMOC to its intensity at the initial glacial state. However, according to *Renold et al.* [2009], under modern conditions the time delay is shorter, showing stage 2 onset before the AMOC has made its initial recovery. This may be an indication that the relationship between the onset time of each stage and the timing of initial AMOC recovery can have an important connection to the climate state.

Acknowledgments. This research was supported by the Paleoclimate Program of NSF, NCAR, DOE, Peking University, Special public sector research of CMA, China (GYHY200906016), and Innovation Plan to Graduate Students in the Universities of Jiangsu Province, China (CX07B_043z) and NUIST (Y602).

REFERENCES

Arzel, O., M. H. England, and W. P. Sijp (2008), Reduced stability of the Atlantic meridional overturning circulation due to wind stress feedback during glacial times, *J. Clim.*, *21*, 6260–6282, doi:10.1175/2008JCLI2291.1.

Barker, S., P. Diz, M. J. Vautravers, J. Pike, G. Knorr, I. R. Hall, and W. S. Broecker (2009), Interhemispheric Atlantic seesaw response during the last deglaciation, *Nature*, *457*, 1097–1102, doi:10.1038/nature07770.

Bentsen, M., H. Drange, T. Furevik, and T. Zhou (2004), Simulated variability of the Atlantic meridional overturning circulation, *Clim. Dyn.*, *22*, 701–720, doi:10.1007/s00382-004-0397-x.

Bitz, C. M., J. C. H. Chiang, W. Cheng, and J. J. Barsugli (2007), Rates of thermohaline recovery from freshwater pulses in modern, Last Glacial Maximum, and greenhouse warming climates, *Geophys. Res. Lett.*, *34*, L07708, doi:10.1029/2006GL029237.

Broecker, W. S. (1990), Salinity history of the northern Atlantic during the last deglaciation, *Paleoceanography*, *5*, 459–467, doi:10.1029/PA005i004p00459.

Carlson, A., D. W. Oppo, R. E. Came, A. N. LeGrande, L. D. Keigwin, and W. B. Curry (2008), Subtropical Atlantic salinity variability and Atlantic meridional circulation during the last deglaciation, *Geology*, *36*(12), 991–994, doi:10.1130/G25080A.

Clarke, P. U., N. G. Pisias, T. F. Stocker, and A. J. Weaver (2002), The role of the thermohaline circulation in abrupt climate change, *Nature*, *415*, 863–869, doi:10.1038/415863a.

Collins, W. D., et al. (2006), The Community Climate System Model version 3 (CCSM3), *J. Clim.*, *19*, 2122–2143, doi:10.1175/JCLI3747.1.

Ganopolski, A., and S. Rahmstorf (2001), Rapid changes of glacial climate simulated in a coupled climate model, *Nature*, *409*, 153–158, doi:10.1038/35051500.

Gent, P. R. (2001), Will the North Atlantic Ocean thermohaline circulation weaken during the 21st century?, *Geophys. Res. Lett.*, *28*, 1023–1026, doi:10.1029/2000GL011727.

Goosse, H., H. Renssen, F. M. Selten, R. J. Haarsma, and J. D. Opsteegh (2002), Potential causes of abrupt climate events: A numerical study with a three-dimensional climate model, *Geophys. Res. Lett.*, *29*(18), 1860, doi:10.1029/2002GL014993.

Hu, A., G. A. Meehl, and W. Han (2007), Role of the Bering Strait in the thermohaline circulation and abrupt climate change, *Geophys. Res. Lett.*, *34*, L05704, doi:10.1029/2006GL028906.

Hu, A., B. L. Otto-Bliesner, G. A. Meehl, W. Han, C. Morrill, E. Brady, and B. P. Briegleb (2008), Response of thermohaline circulation to freshwater forcing under present day and LGM conditions, *J. Clim.*, *21*, 2239–2258, doi:10.1175/2007JCLI1985.1.

Knorr, G., and G. Lohmann (2003), Southern Ocean origin for the resumption of Atlantic thermohaline circulation during deglaciation, *Nature*, *424*, 532–536, doi:10.1038/nature01855.

Knutti, R., J. Fluckiger, T. F. Stocker, and A. Timmermann (2004), Strong hemispheric coupling of glacial climate through freshwater discharge and ocean circulation, *Nature*, *430*, 851–856, doi:10.1038/nature02786.

Krebs, U., and A. Timmermann (2007a), Fast advective recovery of the Atlantic meridional overturning circulation after a Heinrich event, *Paleoceanography*, *22*, PA1220, doi:10.1029/2005PA001259.

Krebs, U., and A. Timmermann (2007b), Tropical air–sea interactions accelerate the recovery of the Atlantic meridional overturning circulation after a major shutdown, *J. Clim.*, *20*, 4940–4956, doi:10.1175/JCLI4296.1.

Latif, M., C. Böning, J. Willebrand, A. Biastoch, J. Dengg, N. Keenlyside, U. Schweckendiek, and G. Madec (2006), Is the thermohaline circulation changing?, *J. Clim.*, *19*, 4631–4637, doi:10.1175/JCLI3876.1.

Levermann, A., A. Griesel, M. Hofmann, M. Montoya, and S. Rahmstorf (2005), Dynamic sea level changes following changes in the thermohaline circulation, *Clim. Dyn.*, *24*, 347–354, doi:10.1007/s00382-004-0505-y.

Lippold, J., J. Grützner, D. Winter, Y. Lahaye, A. Mangini, and M. Christl (2009), Does sedimentary $^{231}Pa/^{230}Th$ from the Bermuda Rise monitor past Atlantic meridional overturning circulation?, *Geophys. Res. Lett.*, *36*, L12601, doi:10.1029/2009GL038068.

Liu, Z., et al. (2009), Transient simulation of last deglaciation with a new mechanism for Bølling-Allerød warming, *Science*, *325*, 310–314, doi:10.1126/science.1171041.

Manabe, S., and R. J. Stouffer (1995), Simulation of abrupt climate change induced by freshwater input to the North Atlantic Ocean, *Nature*, *378*, 165–167, doi:10.1038/378165a0.

Manabe, S., and R. J. Stouffer (1997), Coupled ocean-atmosphere model response to freshwater input: Comparison to Younger Dryas event, *Paleoceanography*, *12*(2), 321–336, doi:10.1029/96PA03932.

McManus, J. F., R. Francois, J. M. Gherardi, L. D. Keigwin, and S. Brown-Leger (2004), Collapse and rapid resumption of Atlantic meridional circulation linked to deglaciation climate changes, *Nature*, *428*, 834–837, doi:10.1038/nature02494.

Mignot, J., and C. Frankignoul (2005), The variability of the Atlantic meridional overturning circulation, the North Atlantic Oscillation, and the El Niño–Southern Oscillation in the Bergen Climate Model, *J. Clim.*, *18*, 2361–2375, doi:10.1175/JCLI3405.1.

Mignot, J., A. Ganopolski, and A. Levermann (2007), Atlantic subsurface temperatures: Response to a shutdown of the overturning circulation and consequences for its recovery, *J. Clim.*, *20*, 4884–4898, doi:10.1175/JCLI4280.1.

Milne, G. A., and J. X. Mitrovica (2008), Searching for eustasy in deglacial sea level histories, *Quat. Sci. Rev.*, *27*, 2292–2302, doi:10.1016/j.quascirev.2008.08.018.

Otto-Bliesner, B. L., E. C. Brady, G. Clauzet, R. Tomas, S. Levis, and Z. Kothavala (2006), Last Glacial Maximum and Holocene climate in CCSM3, *J. Clim.*, *19*, 2526–2544, doi:10.1175/JCLI3748.1.

Rahmstorf, S. (2002), Ocean circulation and climate during the past 120,000 years, *Nature*, *419*, 207–214, doi:10.1038/nature01090.

Renold, M., C. C. Raible, M. Yoshimori, and T. F. Stocker (2009), Simulated resumption of the North Atlantic meridional overturning circulation – Slow basin-wide advection and abrupt local convection, *Quat. Sci. Rev.*, *29*(1), 101–112, doi:10.1016/j.quascirev.2009.11.005.

Schmittner, A., and E. D. Galbraith (2008), Glacial greenhouse gas fluctuations controlled by ocean circulation changes, *Nature*, *456*, 373–376, doi:10.1038/nature07531.

Shin, S.-I., Z. Liu, B. Otto-Bliesner, E. C. Brady, J. E. Kutzbach, and S. Harrison (2003a), A simulation of the Last Glacial Maximum climate using the NCAR-CCSM, *Clim. Dyn.*, *20*, 127–151, doi:10.1007/s00382-002-0260-x.

Shin, S.-I., Z. Liu, B. L. Otto-Bliesner, J. E. Kutzbach, and S. J. Vavrus (2003b), Southern Ocean sea-ice control of the glacial North Atlantic thermohaline circulation, *Geophys. Res. Lett.*, *30*(2), 1096, doi:10.1029/2002GL015513.

Spence, J. P., M. Eby, and A. J. Weaver (2008), The sensitivity of the Atlantic meridional overturning circulation to freshwater forcing at eddy-permitting resolutions, *J. Clim.*, *21*, 2697–2710, doi:10.1175/2007JCLI2103.1.

Stouffer, R. J., et al. (2006), Investigating the causes of the response of the thermohaline circulation to past and future climate changes, *J. Clim.*, *19*, 1365–1387, doi:10.1175/JCLI3689.1.

Vellinga, M., and R. A. Wood (2002), Global climatic impacts of a collapse of the Atlantic thermohaline circulation, *Clim. Change*, *54*, 251–267.

Wright, D. G., and T. F. Stocker (1991), A zonally averaged ocean model for the thermohaline circulation, Part I: Model development and flow dynamics, *J. Phys. Oceanogr.*, *21*, 1713–1724, doi:10.1175/1520-0485(1991)021<1713:AZAOMF>2.0.CO;2.

Yin, J., M. E. Schlesinger, N. G. Andronova, S. Malyshev, and B. Li (2006), Is a shutdown of the thermohaline circulation irreversible?, *J. Geophys. Res.*, *111*, D12104, doi:10.1029/2005JD006562.

E. C. Brady and B. L. Otto-Bliesner, Climate and Global Dynamics Division, National Center for Atmospheric Research, Boulder, CO 80307-3000, USA.

J. Cheng, Key Laboratory of Meteorological Disaster of Ministry of Education and College of Atmospheric Sciences, Nanjing University of Information Science and Technology, Nanjing, 210044, China. (chengjun@nuist.edu.cn)

F. He, Z. Liu, and M. Wehrenberg, Center for Climatic Research and Department of Atmospheric and Oceanic Sciences, University of Wisconsin-Madison, Madison, WI 53706, USA.